

Phase-controllable spin wave generation in iron garnet by linearly polarized light pulses

Isao Yoshimine, Takuya Satoh, Ryugo Iida, Andrzej Stupakiewicz, Andrzej Maziewski, and Tsutomu Shimura

Citation: [Journal of Applied Physics](#) **116**, 043907 (2014); doi: 10.1063/1.4891107

View online: <http://dx.doi.org/10.1063/1.4891107>

View Table of Contents: <http://scitation.aip.org/content/aip/journal/jap/116/4?ver=pdfcov>

Published by the [AIP Publishing](#)



AIP | Journal of
Applied Physics

Journal of Applied Physics is pleased to
announce **André Anders** as its new Editor-in-Chief

Phase-controllable spin wave generation in iron garnet by linearly polarized light pulses

Isao Yoshimine,¹ Takuya Satoh,^{1,2,3,a)} Ryugo Iida,¹ Andrzej Stupakiewicz,⁴ Andrzej Maziewski,⁴ and Tsutomu Shimura¹

¹*Institute of Industrial Science, The University of Tokyo, Tokyo 153-8505, Japan*

²*PRESTO, Japan Science and Technology Agency, Tokyo 102-0076, Japan*

³*Department of Physics, Kyushu University, Fukuoka 812-8581, Japan*

⁴*Laboratory of Magnetism, Faculty of Physics, University of Białystok, Białystok 15-424, Poland*

(Received 26 May 2014; accepted 12 July 2014; published online 24 July 2014)

A phase-controlled spin wave was non-thermally generated in bismuth-doped rare-earth iron garnet by linearly polarized light pulses. We controlled the initial phase of the spin wave continuously within a range of 180° by changing the polarization azimuth of the excitation light. The azimuth dependences of the initial phase and amplitude of the spin wave were attributed to a combination of the inverse Cotton-Mouton effect and photoinduced magnetic anisotropy. Temporally and spatially resolved spin wave propagation was observed with a CCD camera, and the waveform was in good agreement with calculations. A nonlinear effect of the spin excitation was observed for excitation fluences higher than 100 mJ/cm^2 . © 2014 AIP Publishing LLC.

[<http://dx.doi.org/10.1063/1.4891107>]

I. INTRODUCTION

Transportation of spin is a major research topic in two research areas of modern physics that have been attracting considerable attention, namely, spintronics¹ and magnonics.² The spin transportation is mediated by two types of carriers: conduction electrons (spin polarized current) and localized electrons (spin wave). The propagation length of spin polarized current is limited to roughly several hundred nanometers, which is determined by the propagation length of free electrons.³ In contrast, a spin wave can also be generated in insulators, and it is known that the propagation length of a spin wave can be as large as several centimeters in an insulator with a low damping coefficient.⁴ Therefore, magnonics is expected to be a fundamental technology in information transport using spin waves.

In past studies, spin waves were generated by applying microwaves from a microstrip antenna,^{5,6} or by using spin transfer torque.^{7,8} Interference^{9,10} and phase control^{11,12} of spin waves generated by microwaves were realized by using a waveguide on yttrium iron garnet. This phase control was accomplished by spatial modulation of the external magnetic field¹¹ or a change in dispersion due to the amplitude of the spin wave.^{11,12} However, it is necessary to attach electrodes to the sample for this type of spin wave generation, and the spatial waveform of the microwaves or spin current is limited by the shape of the electrodes.

Recently, thermal emission of spin waves using ultra-short light pulses, without the need for electrodes, was studied in Ni (Refs. 13 and 14) and permalloy¹⁴ films. Following this, spin waves were generated non-thermally in bismuth-doped rare-earth iron garnet via the inverse Faraday effect (IFE), and the propagation of spin waves was observed

directly at a probe spot away from the pump spot, where the spin waves were generated.¹⁵

In addition, it is expected that more-arbitrary spin wave emission will be realized by using light pulses. For example, directional control of spin wave propagation by controlling the spot shape of excitation light pulses has been reported.¹⁵ Another promising technique for controlling the spin wavefront is using a phased array, which has been applied to phonon-polaritons.¹⁶ To realize a spin wave phased array, the initial phase of the spin wave must be controlled.

The light pulses used to excite spin precession via the IFE are circularly polarized, and the initial phase of the spin precession is determined by the helicity of the polarization.^{17,18} As a result, the initial phase of the spin waves generated via the IFE is restricted to two phases with a difference of π between them. On the other hand, non-thermal excitation of spin precession by linearly polarized light pulses was reported by Kalashnikova.¹⁹ This spin excitation was described as the generation of an impulsive effective field within the pump spot via the inverse Cotton-Mouton effect (ICME). Spin excitation by linearly polarized light was also reported by Hansteen²⁰ and Atoneche;²¹ they attributed the mechanism of the excited spin precession to photoinduced magnetic anisotropy (PMA). Thus, the physics of spin excitation by linearly polarized light is still not well understood.

In this paper, we present phase-controlled spin wave emission by linearly polarized light pulses. Also, we explain the polarization azimuth dependence of the initial phase and amplitude of the spin precession based on a combination of the ICME and PMA. This paper is organized as follows. In Sec. II, we explain the material in which we generated spin waves and the experimental method of generating and observing spin waves. In Sec. III, we show that the amplitude and initial phase of spin precession excited by linearly polarized light pulses are varied continuously by changing the

^{a)}Electronic mail: satoh@phys.kyushu-u.ac.jp

polarization azimuth of the light pulses. Then, we show that the polarization azimuth dependence is explained by considering both ICME and PMA. In Sec. IV, we observe propagation of a spin wave with a CCD camera and describe how the optically generated spin wave propagates. In Sec. V, we discuss nonlinearity of the spin excitation at high pump fluence.

II. MATERIALS AND METHODS

The sample was $\text{Gd}_{4/3}\text{Yb}_{2/3}\text{BiFe}_5\text{O}_{12}$ (111) containing 10^3 ppm Pb as impurities. The lateral dimensions were $6\text{ mm} \times 6\text{ mm}$, and the thickness was $d = 110\text{ }\mu\text{m}$. This was a single crystal with $m3m$ symmetry. Saturation magnetization of the sample was $M_s = 90\text{ emu/cm}^3$, and the Curie temperature was $T_c = 573\text{ K}$.¹⁵ All experiments were conducted at room temperature. We applied an in-plane external magnetic field of $H_{\text{ext}} = 1\text{ kOe}$. As a result, the sample was in a mono-domain state. The ratio h of the out-of-plane component to the in-plane component of magnetization was measured to be $h = 5 \times 10^{-3}$ from Faraday rotation. For the experimental details, see Ref. 22. $\{x, y, z\}$ -axes are defined as a set of coordinate axes that satisfy the following conditions: the x -axis is parallel to the external magnetic field, and the z -axis is perpendicular to the sample surface. The $\{X, Y, Z\}$ -axes are defined as being parallel to the $[11\bar{2}]$, $[1\bar{1}0]$, and $[111]$ crystallography axis, respectively. The X -axis of the sample was tilted $\psi = -5^\circ$ from the x -axis, as shown in Fig. 1. The initial magnetization \mathbf{M}_0 is $\mathbf{M}_0 = M_s(\hat{x} + h\hat{z})$. The initial effective field \mathbf{H}_0 is the sum of the external magnetic field \mathbf{H}_{ext} , the uniaxial magnetic anisotropy field \mathbf{H}_u , and the demagnetizing field \mathbf{H}_d , that is, $\mathbf{H}_0 = \mathbf{H}_{\text{ext}} + \mathbf{H}_u + \mathbf{H}_d = (H_{\text{ext}} - H_u - 4\pi M_s N_{\parallel})(\hat{x} + h\hat{z}) = H_0(\hat{x} + h\hat{z})$. Here, $H_u = 450\text{ Oe}$ was the magnetic anisotropy field, which has been measured using both magneto-optical magnetometry and ferromagnetic resonance, and $N_{\parallel} = 0.014$ and $N_{\perp} = 0.972$ are demagnetizing factors.²³ Note that $\mathbf{M}_0 = \chi\mathbf{H}_0$, where $\chi = 0.17$. For detailed calculation of \mathbf{M}_0 and \mathbf{H}_0 , see the appendix.

Spin precession excited by linearly polarized light pulses was measured by the pump-probe method. The sample was illuminated perpendicularly to the sample surface by the pump pulses with 1300 nm wavelength,²⁴ and $\tau = 150\text{ fs}$

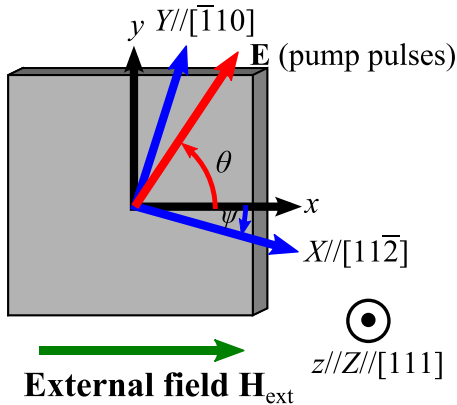


FIG. 1. Definition of coordinate axes, polarization azimuth θ , and crystallographic azimuth ψ . The x -axis is parallel to the external magnetic field.

time duration. The polarization azimuth of the pump pulses was tilted by angle θ from the x -axis (see Fig. 1), and therefore, the electric field amplitude of the pump pulses is $\mathcal{E} = \mathcal{E}_0(\cos\theta\hat{x} + \sin\theta\hat{y})$. Light pulses with 800 nm wavelength, 150 fs time duration, and approximately 7° angle of incidence were used as probe pulses. The probe pulses were linearly polarized. The temporal waveform of spin precession was obtained by measuring the Faraday rotation of probe pulses, which is proportional to the out-of-plane component of the magnetization, at various delays between the pump pulses and probe pulses. We conducted two types of measurements. One is temporally resolved measurement of spin precession at the pump spot. In this experiment, pump pulses with 75 mJ/cm^2 fluence were focused on the sample to a spot diameter of $80\text{ }\mu\text{m}$. The definition of diameter is $2r_0$ in Ref. 15, which is half of the e^{-2} diameter. The probe pulses had a fluence of 0.2 mJ/cm^2 , and their polarization azimuth was tilted by 45° from the x -axis. The probe pulses were focused on the sample to a spot diameter of $30\text{ }\mu\text{m}$. Two orthogonal polarization components of the probe pulses were measured by photodetectors using a balanced detection scheme. The other measurement is spatio-temporally resolved measurement of spin wave propagation. In this experiment, pump pulses with 85 mJ/cm^2 fluence were focused on the sample to a spot diameter of $60\text{ }\mu\text{m}$. A large area of the sample, with a diameter of 5 mm , was illuminated by probe pulses. The probe pulses had a fluence of 0.1 mJ/cm^2 , and their polarization azimuth was along the y -axis. The Faraday rotation of the probe polarization was observed based on the rotating analyzer method using a CCD camera.^{25,26}

III. POLARIZATION AZIMUTH DEPENDENCE OF SPIN PRECESSION

Temporal waveforms of the Faraday rotation of the probe polarization, ϕ_F , at several polarization azimuths of the pump pulses are shown in Fig. 2. These waveforms correspond to spin precession. A temporal waveform oscillating with a frequency of approximately 2.5 GHz was observed. This frequency was independent of the polarization azimuth.

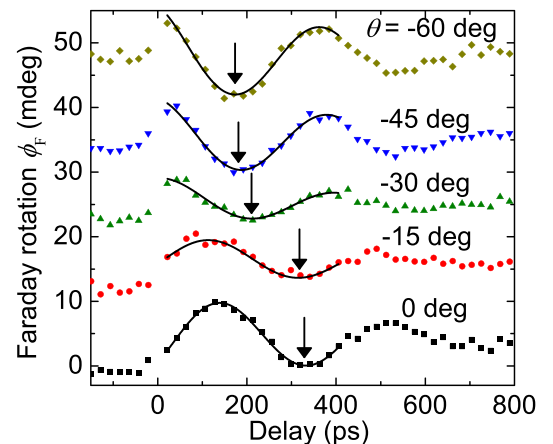


FIG. 2. Temporal waveform of Faraday rotation of probe pulses measured at several polarization azimuths of pump pulses. Black lines show fitting curve given by Eq. (1). Arrows show first negative peak.

It was found that the initial phase of the waveform varied with the polarization azimuth of the pump pulses. This can be confirmed by the shift of the first negative peak, as indicated by arrows in the figure. To extract the initial phase, we fitted the waveforms with the function

$$\phi_F(t) = A \exp(-Bt) \sin(2\pi ft + C) + Dt + E \quad (1)$$

in the range $20 \leq t \leq 400$ ps. We fixed $f = 2.53$ GHz, and set A , B , C , D , and E as fitting parameters. We defined B independently of the polarization azimuth of the pump pulses. As a result of fitting, we obtained $B = 6 \times 10^{-4}$ ps $^{-1}$. The dependences of the amplitude A and initial phase C on the polarization azimuth of the pump pulses θ are presented in Figs. 3(a) and 3(b), respectively. The initial phase was varied continuously, except at $\theta \approx 75^\circ$, where the amplitude was minimized, at nearly zero, and the initial phase jumped by 180° . In addition, the initial phase changed considerably around $\theta \approx -25^\circ$, where the amplitude was a local minimum.

In the following, we discuss the mechanism of photoinduced spin precession. The interaction between light and a spin system can be divided into two phenomena, which have different time scales. One is impulsive generation of an effective field by light pulses, which occurs in a pulse duration that is much shorter than the period of spin precession. The other is a photoinduced change of the effective field, whose relaxation time is much longer than the period of the spin precession. These are analogous to two phenomena that generate a coherent phonon: an impulsive driving force via impulsive stimulated Raman scattering²⁷ and a step function-like driving force via the displacive excitation of coherent phonons,²⁸ respectively.

Here, we discuss magneto-optical interactions that induce these two types of effective fields. First, we focus on ICME, which generates an impulsive effective field. ICME is one of the effects that causes spin precession described as impulsive stimulated Raman scattering.^{17,19,29} The Hamiltonian of ICME induced by linearly polarized light is written using modulation of the dielectric tensor $\delta\epsilon_{ij}$ (Refs. 19, 30, and 31) (where i, j, k , and l denote $\{x, y, z\}$ or $\{X, Y, Z\}$)

$$\mathcal{H}_{\text{ICME}} = -\text{Re} \left[\frac{\delta\epsilon_{ij}}{16\pi} \mathcal{E}_i \mathcal{E}_j^* \delta_\tau(t) \right]. \quad (2)$$

Here, $\delta_\tau(t)$ is an impulse function with width τ , and $\delta\epsilon_{ij}$ is a function of the magnetization \mathbf{M} and modulation of magnetization \mathbf{m} , and is given by^{32,33}

$$\delta\epsilon_{ij} = 2g_{ijkl}(\mathbf{M})_k(\mathbf{m})_l. \quad (3)$$

Here, g is the fourth-rank tensor, which is symmetric over the first pair of indices and over the last pair of indices. The effective field generated by ICME is written as

$$(\mathbf{H}_{\text{ICME}})_l \delta_\tau(t) = -\frac{\partial \mathcal{H}_{\text{ICME}}}{\partial (\mathbf{m})_l} = \frac{1}{8\pi} g_{ijkl}(\mathbf{M})_k \mathcal{E}_i \mathcal{E}_j^* \delta_\tau(t). \quad (4)$$

Next, we focus on PMA, whose decay to its equilibrium value is negligible. PMA energy can be written as^{20,34,35}

$$W_{\text{PMA}}(t) = -\frac{1}{16\pi} a_{ijkl}(\mathbf{M})_k(\mathbf{M})_l \mathcal{E}_i \mathcal{E}_j^* \int_{-\infty}^t \delta_\tau(t') dt'. \quad (5)$$

Therefore, the effective field \mathbf{H}_{PMA} induced by PMA is expressed as

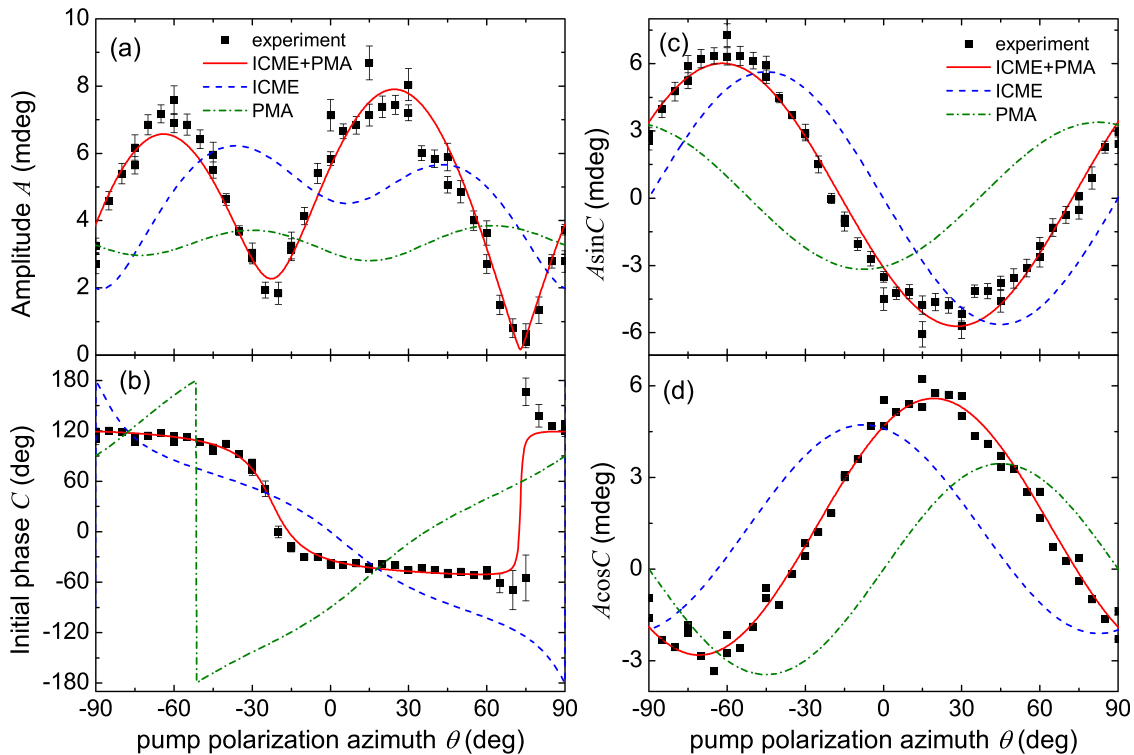


FIG. 3. Polarization dependence of (a) amplitude A , (b) initial phase C , (c) $A \sin C$, and (d) $A \cos C$. Red solid lines are fitting curves using Eqs. (16a) and (16b). Blue broken line and green dashed line indicate the contributions of ICME and PMA, respectively.

$$\begin{aligned}
 (\mathbf{H}_{\text{PMA}})_I \int_{-\infty}^t \delta_\tau(t') dt' &= -\frac{\partial W_{\text{PMA}}}{\partial (\mathbf{M})_I} \\
 &= \frac{1}{8\pi} a_{ijkl} (\mathbf{M}_0)_k \mathcal{E}_i \mathcal{E}_j^* \int_{-\infty}^t \delta_\tau(t') dt'.
 \end{aligned} \quad (6)$$

In iron garnets, photoinduced redistribution of electrons between nonequivalent Fe ions in octahedral and tetrahedral sites³⁶ or impurity Pb ions³⁷ may cause a change in the magnetocrystalline anisotropy, which leads to PMA. Reduction of electrons whose polarization is parallel to the optical polarization by selective excitation is known to be a mechanism of PMA induced by linearly polarized light.³⁸ a_{ijkl} is tensor that determines PMA, and non-zero components are determined by the symmetry of anisotropic sites in the crystal.

Impulsive generation of the effective field by ICME contributes to spin precession in the form of an instantaneous displacement of the magnetization \mathbf{M} . On the other hand, the generation of a step function-like effective field by PMA contributes to the spin precession as an instantaneous change of the effective field \mathbf{H}_{eff} . Here, we assume $\mathbf{H}_{\text{ICM}} \gg \mathbf{H}_{\text{PMA}}$. Under the impulsive effective field \mathbf{H}_{ICM} , the dynamics of the magnetization \mathbf{M} are as follows:

$$\frac{d\mathbf{M}}{dt} = -\gamma(\mathbf{M} \times \mathbf{H}_{\text{ICM}}). \quad (7)$$

Here, $\gamma = 2.8 \text{ MHz/Oe}$ is the gyromagnetic ratio, and $\mathbf{M}(t = \tau)$ is

$$\mathbf{M}(t = \tau) = \mathbf{M}_0 - \tau\gamma(\mathbf{M}_0 \times \mathbf{H}_{\text{ICM}}). \quad (8)$$

The effective field at $t \geq \tau$, \mathbf{H}_{eff} , is expressed as

$$\mathbf{H}_{\text{eff}} = \mathbf{H}_0 + \mathbf{H}_{\text{PMA}}. \quad (9)$$

The dynamics of the magnetization and effective field are illustrated in Fig. 4.

Then, we introduce vectors \mathbf{u}_1 , \mathbf{u}_2 , and \mathbf{u}_3 . We define \mathbf{u}_1 as a component of $\mathbf{M}(t = \tau)$ that is perpendicular to \mathbf{H}_{eff} , and \mathbf{u}_3 as a component of $\mathbf{M}(t = \tau)$ that is parallel to \mathbf{H}_{eff} . We define \mathbf{u}_2 satisfying conditions $|\mathbf{u}_1| = |\mathbf{u}_2|$, $\mathbf{u}_2 \perp \mathbf{H}_{\text{eff}}$, and

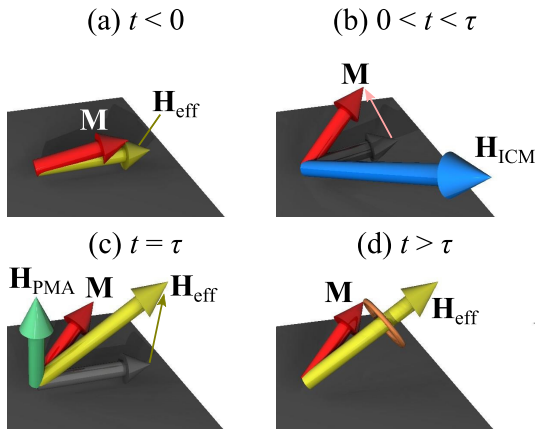


FIG. 4. Dynamics of magnetization and effective field at (a) $t < 0$, (b) $0 < t < \tau$, (c) $t = \tau$, and (d) $t > \tau$.

$\mathbf{u}_2 \perp \mathbf{M}(t = \tau)$. These vectors are schematically illustrated in Fig. 5. Using \mathbf{u}_1 , \mathbf{u}_2 , and \mathbf{u}_3 , the magnetization $\mathbf{M}(t \geq \tau)$ precessing around \mathbf{H}_{eff} is written as

$$\mathbf{M}(t \geq \tau) = \mathbf{u}_1 \cos 2\pi ft + \mathbf{u}_2 \sin 2\pi ft + \mathbf{u}_3. \quad (10)$$

Here,

$$\mathbf{u}_1 = \mathbf{M}(t = \tau) - \frac{\mathbf{M}(t = \tau) \cdot \mathbf{H}_{\text{eff}}}{|\mathbf{H}_{\text{eff}}|^2} \mathbf{H}_{\text{eff}}, \quad (11a)$$

$$\mathbf{u}_2 = -\frac{\mathbf{M}(t = \tau) \times \mathbf{H}_{\text{eff}}}{|\mathbf{H}_{\text{eff}}|}, \quad (11b)$$

$$\mathbf{u}_3 = \frac{\mathbf{M}(t = \tau) \cdot \mathbf{H}_{\text{eff}}}{|\mathbf{H}_{\text{eff}}|^2} \mathbf{H}_{\text{eff}}. \quad (11c)$$

We can make the approximation that \mathbf{u}_1 , \mathbf{u}_2 , \mathbf{u}_3 are constant vectors because the decay of \mathbf{H}_{PMA} is negligible. Faraday rotation of the probe pulses, ϕ_F , is proportional to the z -component of the magnetization $(\mathbf{M})_z$

$$\phi_F = F(\mathbf{M})_z. \quad (12)$$

Here, $F = 880 \text{ m deg} \cdot \text{cm}^3/\text{emu}$ was obtained from static Faraday rotation.²² Comparing Eqs. (1), (10), and (12) yields

$$F(\mathbf{u}_1)_z = A \sin C, \quad (13a)$$

$$F(\mathbf{u}_2)_z = A \cos C. \quad (13b)$$

Here, we neglect $\exp(-Bt)$ in Eq. (1), which corresponds to relaxation of spin precession. Polarization dependences of $A \sin C$ and $A \cos C$ are plotted in Figs. 3(c) and 3(d).

Here, we derive \mathbf{H}_{ICM} and \mathbf{H}_{PMA} to clarify the polarization azimuth dependence of the magnetization dynamics. From Eq. (4), in the crystal with symmetry $m3m$, we have

$$\begin{aligned}
 (\mathbf{H}_{\text{ICM}})_x &= -\frac{\chi \mathcal{E}_0^2 H_0}{8\pi} \left[\frac{1}{2}(g_1 + g_2) + \frac{1}{2}(g_1 - g_2) \cos 2\theta \right. \\
 &\quad \left. - h g_3 \cos(2\theta - 3\psi) \right],
 \end{aligned} \quad (14a)$$

$$\begin{aligned}
 (\mathbf{H}_{\text{ICM}})_y &= -\frac{\chi \mathcal{E}_0^2 H_0}{8\pi} \left[\frac{1}{2}(g_1 - g_2) \sin 2\theta + h g_3 \sin(2\theta - 3\psi) \right],
 \end{aligned} \quad (14b)$$

$$\begin{aligned}
 (\mathbf{H}_{\text{ICM}})_z &= \frac{\chi \mathcal{E}_0^2 H_0}{8\pi} [-g_3 \cos(2\theta - 3\psi) + h g_4].
 \end{aligned} \quad (14c)$$

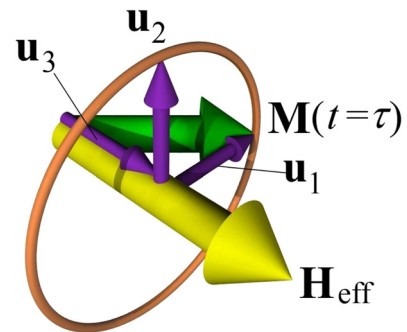


FIG. 5. Definition of \mathbf{u}_1 , \mathbf{u}_2 , and \mathbf{u}_3 . \mathbf{u}_1 and \mathbf{u}_3 were defined to fulfill the conditions $\mathbf{u}_1 + \mathbf{u}_3 = \mathbf{M}(t = \tau)$ and $\mathbf{u}_3 \parallel \mathbf{H}_{\text{eff}}$. \mathbf{u}_2 was defined to fulfill the conditions $|\mathbf{u}_1| = |\mathbf{u}_2|$ and $\mathbf{u}_1 \perp \mathbf{u}_2$.

Here,

$$g_{XXXX} = g_{YYYY} = g_1, \quad (15a)$$

$$g_{XXYY} = g_{YYXX} = g_2, \quad (15b)$$

$$g_{YYZX} = g_{ZXYY} = -g_{ZXXX} = -g_{XXZX} \\ = g_{YZXY} = g_{XYYZ} = g_3, \quad (15c)$$

$$g_{ZZXX} = g_{ZZYY} = g_{XXZZ} = g_{YYZZ} = g_4 \\ = -\frac{4}{21}g_1 + \frac{4}{3}g_2 + \frac{\sqrt{2}}{21}g_3, \quad (15d)$$

$$g_{XYXY} = \frac{1}{2}(g_1 - g_2). \quad (15e)$$

\mathbf{H}_{PMA} can be obtained by replacing g_i with a_i in Eqs. (14a)–(14c), because a_{ijkl} has the same non-zero components as g_{ijkl} .

Then, we calculate the component of $A \sin C$ and $A \cos C$ that is proportional to the intensity of pump pulses $I = (nc/8\pi)\mathcal{E}_0^2$, neglecting higher order terms of I . We end up with

$$A \sin C = F(\mathbf{u}_1)_z \\ = -I \frac{F\chi^2 H_0}{nc} \left[\left(\tau\gamma H_0 \frac{1}{2}(g_1 - g_2) \right) \sin 2\theta \right. \\ + \tau\gamma H_0 h g_3 \sin(2\theta - 3\psi) - a_3 \cos(2\theta - 3\psi) \\ \left. + \left(\frac{h}{2}(a_1 - a_2) \right) \cos 2\theta + \left(\frac{h}{2}(a_1 + a_2) + ha_4 \right) \right], \quad (16a)$$

$$A \cos C = F(\mathbf{u}_2)_z \\ = -I \frac{F\chi^2 H_0}{nc} \left[\left(\frac{1}{2}(a_1 - a_2) \right) \sin 2\theta \right. \\ + ha_3 \sin(2\theta - 3\psi) + \tau\gamma H_0 g_3 \cos(2\theta - 3\psi) \\ + \left(\tau\gamma H_0 \frac{h}{2}(g_1 - g_2) \right) \cos 2\theta \\ \left. + \tau\gamma H_0 \left(\frac{h}{2}(g_1 + g_2) - hg_4 \right) \right]. \quad (16b)$$

Here, we neglected terms of order h^2 and postulated that $H_0 \gg |\mathbf{H}_{\text{PMA}}|$. We fitted the polarization azimuth dependence of $A \sin C$ and $A \cos C$ using Eqs. (16a) and (16b). The results are shown in Figs. 3(c) and 3(d) (red lines). When we take into account both ICME and PMA, we can identify parameters that determine ICME and PMA, namely, g_1 , g_2 , g_3 , a_1 , a_2 , and a_3 from the fitting. On the other hand, when we take into account ICME ($a_{ijkl} = 0$) or PMA ($g_{ijkl} = 0$) alone, we cannot obtain a good fit for the experimental results shown in Fig. 3. Therefore, the polarization azimuth dependence of $(\mathbf{u}_1)_z$ and $(\mathbf{u}_2)_z$ can only be described assuming both ICME and PMA, not just one of them.

From the fitting, we estimated $|\mathbf{H}_{\text{ICM}}|$ and $|\mathbf{H}_{\text{PMA}}|$ to be $|\mathbf{H}_{\text{ICM}}| \approx 80 \text{ kOe}$, and $|\mathbf{H}_{\text{PMA}}| \approx 1 \text{ Oe}$. The estimated value of $|\mathbf{H}_{\text{PMA}}|$ is consistent with the previously reported result.²⁰ Here, we confirm the assumption $|\mathbf{H}_{\text{ICM}}| \gg H_0 \gg |\mathbf{H}_{\text{PMA}}|$. Because $H_0 \gg |\mathbf{H}_{\text{PMA}}|$, \mathbf{H}_{PMA} does not affect the frequency of spin precession, which agrees with the experimental result. We also estimated the parameters g_1, g_2, g_3, a_1, a_2 , and a_3 from the fitting. The parameter g_3 was three orders of magnitude smaller than g_1, g_2 , and g_4 . Therefore, considering

Eqs. (14a)–(14c), the x -component is dominant for \mathbf{H}_{ICM} . On the other hand, a_1, a_2, a_3 , and a_4 are comparable, and thus, the x, y , and z -components are comparable for \mathbf{H}_{PMA} . From the estimation of g_1, g_2, g_3, a_1, a_2 , and a_3 , we conclude the following. When spins are excited by ICME, the spins see the crystal as being spherically symmetric. However, PMA, which occurs with the excitation of ions and the redistribution of electrons, is affected by the symmetry of the crystal.

The contributions of ICME and PMA from the values of g and a are separately shown in Fig. 3. We found that the contributions of ICME and PMA are comparable. The ICME and PMA components change their initial phase continuously in a 360° range as a function of the polarization azimuth, and they have opposite polarization azimuth dependence. Integrating $A \sin C$ and $A \cos C$ with respect to θ in Figs. 3(c) and 3(d) yields non-zero values due to the presence of $h = 5 \times 10^{-3}$. Therefore, even unpolarized femtosecond light pulses can also be used to induce the ICME and PMA.

The resulting initial phase of spin precession is varied within a range of 180° because of interference of the two effects. At $\theta \approx 75^\circ$, the contributions of ICME and PMA cancel each other out, and the amplitude of the spin precession becomes nearly zero. Moreover, the contribution of ICME becomes higher than the contribution of PMA at $\theta \approx 75^\circ$, explaining the observed jump in the initial phase of the spin precession. At $\theta \approx -25^\circ$, the amplitude of spin precession also becomes a local minimum because of destructive interference. On the other hand, at $\theta \approx 20^\circ$ and $\theta \approx -75^\circ$, the contributions of ICME and PMA reinforce each other, and the amplitude becomes maximum.

From Eqs. (16a) to (16b), we make two remarks. One is that the constant components with respect to θ in Figs. 3(c) and 3(d) originate from the non-zero out-of-plane magnetization h . The other is that the polarization azimuth dependences of the amplitude and initial phase depend on the crystal orientation. This is indicated by the ψ -dependence of the equations. Because the absolute value of $\tau\gamma H_0 \frac{1}{2}(g_1 - g_2)$, $\tau\gamma H_0 g_3$, $\frac{1}{2}(a_1 - a_2)$, a_3 are all on the order of 1 mdeg and $h = 5 \times 10^{-3} \ll 1$, the components $\tau\gamma H_0 h g_3 \sin(2\theta - 3\psi)$ and $(h/2)(a_1 - a_2) \cos 2\theta$ in Eq. (16a), and the components $ha_3 \sin(2\theta - 3\psi)$ and $(\tau\gamma H_0 h/2)(g_1 - g_2) \cos 2\theta$ in (16b) are negligible. Therefore, if $\psi = 30 + 60n \text{ deg}$ (n is an integer), for example, if the external field is applied along $[\bar{1}10]$ axis, the initial phase of the spin wave does not change by the polarization azimuth.

The polarization dependence of the initial phase and amplitude can be controlled by suitably designing g_{ijkl} , a_{ijkl} and ψ . The initial phase and amplitude of the spin precession can be visualized by the polar angle and radius of each spot, respectively, on a $(\mathbf{u}_1)_z$ vs. $(\mathbf{u}_2)_z$ plot. As an example, if a $(\mathbf{u}_1)_z$ vs. $(\mathbf{u}_2)_z$ plot shows a circle centered at $(0, 0)$, the initial phase only (keeping the amplitude constant) can be controlled by the polarization azimuth of the pump pulses.

IV. PROPAGATION OF SPIN WAVES GENERATED BY LINEARLY POLARIZED LIGHT PULSES

We observed the spatio-temporal waveform using a CCD camera to examine the propagation of the spin wave

generated by linearly polarized light pulses. We obtained a spatial map of the Faraday rotation of probe pulses transmitted through the sample for various time delays. Using a CCD camera, we obtained the spatial waveform with 5-times higher resolution and 50-times faster speed than the scanning technique.¹⁵ The experimental result at $t = 1400$ ps is exemplified in Fig. 6(a), where only the oscillating component is plotted. According to the result, the wavefronts of the spin waves travel toward the pump spot. This is a characteristic of a backward volume magnetostatic wave (BVMSW).³⁹ Next, we calculated the waveform of the spin wave using the following equation:

$$M_z(\mathbf{r}, t) \propto \int H_{\text{init}}(\mathbf{k}) \sin(\mathbf{k} \cdot \mathbf{r} - \omega(\mathbf{k})t) \exp(-\alpha\omega(\mathbf{k})t) d\mathbf{k}. \quad (17)$$

Here, the source of the spin wave $H_{\text{init}}(\mathbf{k})$ was determined by the Fourier transform of the spatial intensity distribution of the pump spot $|E(r)|^2 \approx \exp(-r^2/2r_0^2)$, and the dispersion curve $\omega(\mathbf{k})$ of the lowest mode of a BVMSW (Ref. 15) was used. The best fit with the experimental result in the range $t \leq 2000$ ps was obtained for a pump spot diameter of $60 \mu\text{m}$, $H_{\text{ext}} = 1$ kOe, $M_s = 1300/4\pi \text{ emu/cm}^3$, $H_u = 600$ Oe, Gilbert damping $\alpha = 0.02$,⁴⁰ $d = 110 \mu\text{m}$, and initial phase $C = 120^\circ$. The calculated spatial plot at $t = 1400$ ps is shown in Fig. 6(b). The good agreement suggests that the

spin wave generated by the linearly polarized light pulses propagates as a BVMSW. Negligible attenuation of the pump pulse along the sample normal may yield effective excitation of a uniform spin wave, such as the lowest order of the BVMSW. Furthermore, the contribution of any surface wave to the Faraday rotation of the probe pulse is negligible compared with that contribution of the volume wave.

Therefore, interference of the spin waves can be expressed as a linear superposition of BVMSWs from different sources. Thus, we can arrange a phased array of spin waves generated by linearly polarized light pulses and estimate the waveform of the spin wave generated by the phased array by calculating a superposition of BVMSWs, although this is out of the scope of this paper.

V. SPIN PRECESSION GENERATED BY LIGHT PULSES WITH HIGH FLUENCE

We measured the polarization azimuth dependences of the amplitude and initial phase of spin precession at several pump fluences, as shown in Figs. 7 and 8, respectively. The frequency of the spin wave did not change. On the other hand, a component that is proportional to $\sin 4\theta$ was observed for pump fluences higher than 100 mJ/cm^2 (see Fig. 7). Saturated absorption by Fe or Pb ions cannot reproduce the $\sin 4\theta$ -component. A nonlinear effect with a quadratic dependence on the pump intensity seems to show up for higher fluence. However, I^2 terms in $(\mathbf{u}_1)_z$ and $(\mathbf{u}_2)_z$, which were neglected in Eqs. (16a) and (16b), could not reproduce the experimental result. Then, we must consider mechanisms that do not occur in the linear region. Further investigation is required.

VI. CONCLUSION

We excited a spin wave whose amplitude and initial phase depended on the polarization azimuth of linearly

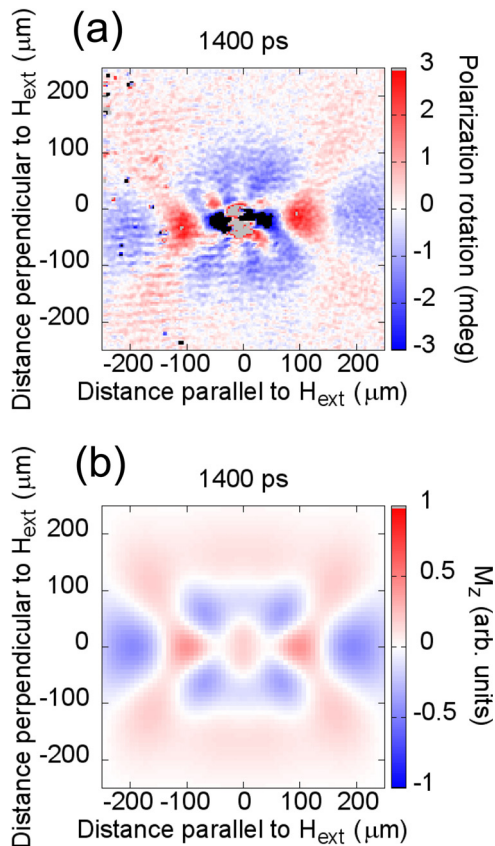


FIG. 6. (a) Experimental spatial plot of spin wave propagation. Polarization azimuth of pump pulses was $\theta = -60^\circ$. The spin wave was emitted at $(0, 0)$. (b) Calculated spatial plot using the dispersion curve of BVMSW. In both figures, plots at the delay $t = 1400$ ps are shown. In the movies, wavefronts travelling inward, which is a characteristic of BVMSW, are shown. (Multimedia view) [URL: <http://dx.doi.org/10.1063/1.4891107.1>]

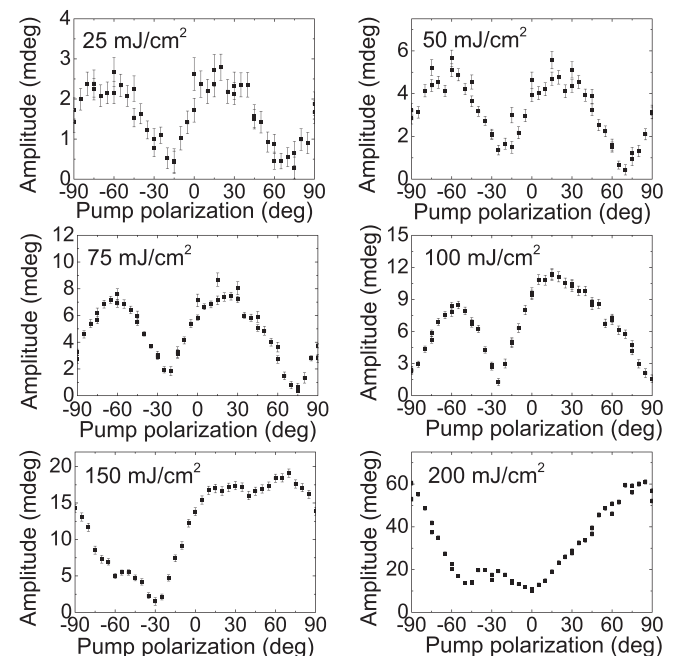


FIG. 7. Polarization azimuth dependence of amplitude of spin precession at pump spot for several pump fluences.

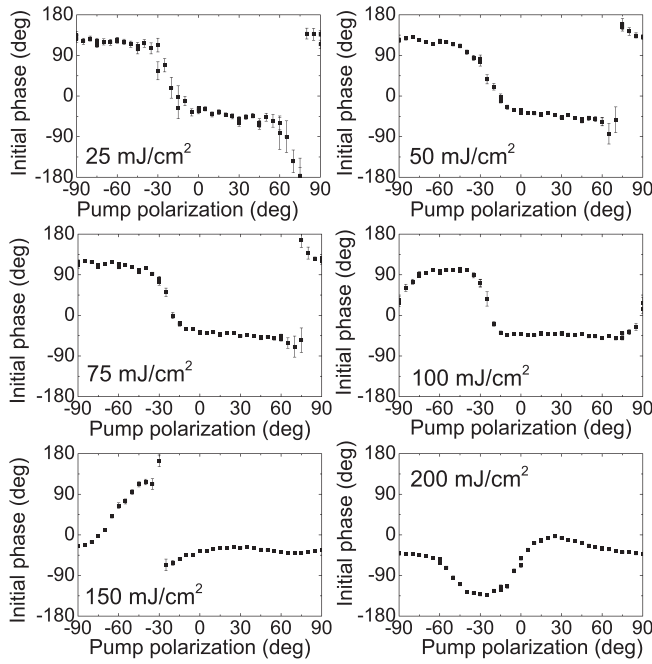


FIG. 8. Polarization azimuth dependence of initial phase of spin precession at pump spot for several pump fluences.

polarized pump pulses. In this sample, the initial phase was varied in a 180° range. We characterized the polarization azimuth dependence of the spin precession based on a combination of the ICME and PMA, as shown in Eqs. (16a) and (16b). Here, the directions of the external field and the magnetization play important roles.

We observed propagation of the spin wave using a CCD camera. From the spatiotemporal waveform of the spin wave, we confirmed that the spin wave generated by linearly polarized light propagates as a BVMSW. Thus, the spin precession induced by linearly polarized light pulses can be used as sources of a phased array of spin waves, which enables shaping of spin waves.

We also found that a nonlinear effect affects the amplitude or initial phase of the spin wave for pump fluences higher than 100 mJ/cm^2 .

ACKNOWLEDGMENTS

The authors would like to thank Y. Terui and Y. Hashimoto for discussions about spin wave propagation and experimental techniques. This work was supported by the Japan Science and Technology Agency (JST)—Precursory Research for Embryonic Science and Technology (PRESTO), KAKENHI (23104706), and the Murata Science Foundation. A.S. acknowledges the financial support of the National Science Centre Poland for Project No. DEC-2013/09/B/ST3/02669.

APPENDIX: CALCULATION OF \mathbf{M}_0 AND \mathbf{H}_0

In this section, the magnetization \mathbf{M}_0 and effective field \mathbf{H}_0 before the sample is illuminated by a pump pulse are calculated. The magnetization can be calculated by minimizing the sum of the uniaxial anisotropy energy

$$W_u = \frac{M_s H_u}{2} \sin^2 \xi, \quad (\text{A1})$$

the Zeeman energy

$$W_{\text{ext}} = -H_{\text{ext}} M_s \sin \xi \cos(\psi - \eta), \quad (\text{A2})$$

and the demagnetizing energy

$$W_d = 2\pi M_s^2 (N_{\parallel} \sin^2 \xi + N_{\perp} \cos^2 \xi). \quad (\text{A3})$$

Here, ξ and η are defined by the azimuth of the magnetization as

$$\mathbf{M}_0 = M_s (\sin \xi \cos \eta \hat{\mathbf{X}} + \sin \xi \sin \eta \hat{\mathbf{Y}} + \cos \xi \hat{\mathbf{Z}}). \quad (\text{A4})$$

The minimum of the total energy is obtained for $\eta = \psi$, $\xi = \arcsin(H_{\text{ext}}/H_u^*)$. Here, $H_u^* = H_u + 4\pi M_s (N_{\parallel} - N_{\perp})$. If $H_{\text{ext}} > H_u^*$, we have $\xi = \pi/2$.

The initial effective field \mathbf{H}_0 is calculated as

$$\begin{aligned} (\mathbf{H}_0)_{\parallel} &= -\frac{\partial(W_u + W_{\text{ext}} + W_d)}{\partial M_{\parallel}} \\ &= H_{\text{ext}} - H_u \sin \xi - 4\pi M_s N_{\parallel} \sin \xi. \end{aligned} \quad (\text{A5a})$$

$$\begin{aligned} (\mathbf{H}_0)_{\perp} &= -\frac{\partial(W_u + W_{\text{ext}} + W_d)}{\partial M_{\perp}} \\ &= -4\pi M_s N_{\perp} \cos \xi. \end{aligned} \quad (\text{A5b})$$

For the sample we used, ξ should be $\xi = \pi/2$ when $H_{\text{ext}} = 1 \text{ kOe}$ because $H_{\text{ext}} > H_u^*$. However, another experimental fact shows that \mathbf{M}_0 has an out-of-plane component, which is 0.5% of the in-plane component ($\cos \xi = h = 5 \times 10^{-3}$). Then, we set the directions of \mathbf{M}_0 and \mathbf{H}_0 as parallel to the vector $(\hat{\mathbf{x}} + 0.005\hat{\mathbf{z}})$.

¹S. A. Wolf, D. D. Awschalom, R. A. Buhrman, J. M. Daughton, S. von Molnár, M. L. Roukes, A. Y. Chtchelkanova, and D. M. Treger, *Science* **294**, 1488 (2001).

²S. O. Demokritov and A. N. Slavin, *Magnonics: From Fundamentals to Applications* (Springer, Berlin, 2013).

³J. Bass and W. P. Pratt, Jr., *J. Phys.: Condens. Matter* **19**, 183201 (2007).

⁴T. Schneider, A. A. Serga, B. Leven, B. Hillebrands, R. L. Stamps, and M. P. Kostylev, *Appl. Phys. Lett.* **92**, 022505 (2008).

⁵S. Tamaru, J. A. Bain, R. J. M. van de Veerdonk, T. M. Crawford, M. Covington, and M. H. Kryder, *J. Appl. Phys.* **91**, 8034 (2002).

⁶A. A. Serga, A. V. Chumak, and B. Hillebrands, *J. Phys. D* **43**, 264002 (2010).

⁷J. C. Slonczewski, *J. Magn. Magn. Mater.* **159**, L1 (1996).

⁸L. Berger, *Phys. Rev. B* **54**, 9353 (1996).

⁹S. Choi, K.-S. Lee, and S.-K. Kim, *Appl. Phys. Lett.* **89**, 062501 (2006).

¹⁰K. Perzlmaier, G. Woltersdorf, and C. H. Back, *Phys. Rev. B* **77**, 054425 (2008).

¹¹U.-H. Hansen, V. E. Demidov, and S. O. Demokritov, *Appl. Phys. Lett.* **94**, 252502 (2009).

¹²A. B. Ustinov, B. A. Kalinikos, and E. Lähderanta, *J. Appl. Phys.* **113**, 113904 (2013).

¹³B. Lenk, G. Eilers, J. Hamrle, and M. Münzenberg, *Phys. Rev. B* **82**, 134443 (2010).

¹⁴M. van Kampen, C. Jozsa, J. T. Kohlhepp, P. LeClair, L. Lagae, W. J. M. de Jonge, and B. Koopmans, *Phys. Rev. Lett.* **88**, 227201 (2002).

¹⁵T. Satoh, Y. Terui, R. Moriya, B. A. Ivanov, K. Ando, E. Saitoh, T. Shimura, and K. Kuroda, *Nature Photon.* **6**, 662 (2012).

¹⁶T. Feurer, J. C. Vaughan, and K. A. Nelson, *Science* **299**, 374 (2003).

¹⁷A. Kirilyuk, A. V. Kimel, and Th. Rasing, *Rev. Mod. Phys.* **82**, 2731 (2010).

- ¹⁸A. V. Kimel, A. Kirilyuk, P. A. Usachev, R. V. Pisarev, A. M. Balbashov, and Th. Rasing, *Nature* **435**, 655 (2005).
- ¹⁹A. M. Kalashnikova, A. V. Kimel, R. V. Pisarev, V. N. Gridnev, P. A. Usachev, A. Kirilyuk, and Th. Rasing, *Phys. Rev. B* **78**, 104301 (2008).
- ²⁰F. Hansteen, A. Kimel, A. Kirilyuk, and Th. Rasing, *Phys. Rev. B* **73**, 014421 (2006).
- ²¹F. Atoneche, A. M. Kalashnikova, A. V. Kimel, A. Stupakiewicz, A. Maziewski, A. Kirilyuk, and Th. Rasing, *Phys. Rev. B* **81**, 214440 (2010).
- ²²S. Parchenko, A. Stupakiewicz, I. Yoshimine, T. Satoh, and A. Maziewski, *Appl. Phys. Lett.* **103**, 172402 (2013).
- ²³S. Chikazumi, *Physics of Ferromagnetism*, 2nd ed. (Oxford University Press, 2009).
- ²⁴The reason for selecting 1300 nm was to suppress the absorption of the pump pulse in the sample and to avoid a temperature increase and damage to the sample due to laser heating. See Supplementary Information in Ref. 15.
- ²⁵A. Laraoui, M. Albrecht, and J. Y. Bigot, *Opt. Lett.* **32**, 936 (2007).
- ²⁶Y. Hashimoto, A. R. Khorsand, M. Savoini, B. Koene, D. Bossini, A. Tsukamoto, A. Itoh, Y. Ohtsuka, K. Aoshima, A. V. Kimel, A. Kirilyuk, and Th. Rasing, *Rev. Sci. Instrum.* **85**, 063702 (2014).
- ²⁷Y.-X. Yan, E. B. Gamble, Jr., and K. A. Nelson, *J. Chem. Phys.* **83**, 5391 (1985).
- ²⁸H. J. Zeiger, J. Vidal, T. K. Cheng, E. P. Ippen, G. Dresselhaus, and M. S. Dresselhaus, *Phys. Rev. B* **45**, 768 (1992).
- ²⁹R. Iida, T. Satoh, T. Shimura, K. Kuroda, B. A. Ivanov, Y. Tokunaga, and Y. Tokura, *Phys. Rev. B* **84**, 064402 (2011).
- ³⁰V. N. Gridnev, *Phys. Rev. B* **77**, 094426 (2008).
- ³¹P. S. Pershan, J. P. van der Ziel, and L. D. Malmstrom, *Phys. Rev.* **143**, 574 (1966).
- ³²V. V. Eremenko, Y. G. Litvinenko, N. K. Kharchenko, and V. M. Naumenko, *Magneto-Optic Effects in Non-Centroantisymmetrical Antiferromagnetic Crystals* (Springer, New York, 1992).
- ³³M. G. Cottam and D. J. Lockwood, *Light Scattering in Magnetic Solids* (Wiley-Interscience, 1986).
- ³⁴A. Stupakiewicz, A. Maziewski, I. Davidenko, and V. Zablotskii, *Phys. Rev. B* **64**, 064405 (2001).
- ³⁵A. B. Chizhik, I. I. Davidenko, A. Maziewski, and A. Stupakiewicz, *Phys. Rev. B* **57**, 14366 (1998).
- ³⁶R. W. Teale, D. W. Temple, U. Enz, and R. F. Pearson, *J. Appl. Phys.* **40**, 1435 (1969).
- ³⁷G. B. Scott and J. L. Page, *J. Appl. Phys.* **48**, 1342 (1977).
- ³⁸E. L. Nagaev, *Phys. Status Solidi B* **145**, 11 (1988).
- ³⁹R. W. Damon and H. V. D. Vaart, *J. Appl. Phys.* **36**, 3453 (1965).
- ⁴⁰The 0.02 value was measured by means of the stripe-FMR and classical FMR (X-band) methods.